Bull. Mater. Sci., Vol. 40, No. 5, September 2017, pp. 887–895
DOI 10.1007/s12034-017-1439-4

Structural, microstructural and optical properties of Cu_2ZnSnS_4 thin films prepared by thermal evaporation: effect of substrate temperature and annealing

U CHALAPATHI[1,2,*], S UTHANNA[1] and V SUNDARA RAJA[1]

[1]Department of Physics, Sri Venkateswara University, Tirupati 517502, India

[2]*Present address* Department of Electronic Engineering, Yeungnam University, 280 Daehak-ro, Gyeongsan-si, Gyeongsangbuk-do, South Korea

*Author for correspondence (chalam.uppala@gmail.com)

MS received 20 July 2016; accepted 5 December 2016; published online 5 August 2017

Abstract. Thin films of Cu_2ZnSnS_4 (CZTS), a promising solar cell absorber, were grown by thermal evaporation of ZnS, Sn and Cu precursors and subsequent annealing in sulphur atmosphere. Two aspects are chosen for investigation: (i) the effect of substrate temperature (T_S) used for the deposition of precursors and (ii) (N_2+S_2) pressure during annealing, to study their impact on the growth of CZTS films. X-ray diffraction analysis of these films revealed the structure to be kesterite with (112) preferred orientation. Crystallite size is found to slightly increase with increase in T_S as well as pressure during annealing. From optical absorption studies, the direct optical band gap of CZTS films is found to be ∼1.45 eV. Room temperature electrical resistivity of the films obtained on annealing the stacks at 10 and 100 mbar pressures is found to be in the ranges 25–55 and 5–25 Ω cm, respectively, depending on T_S. Films prepared by annealing the stack deposited at 300°C under 100 mbar pressure for 90 min are slightly Cu-poor and Zn-rich with compact grain morphology.

Keywords. CZTS thin films; thermal evaporation; annealing; Raman spectroscopy; X-ray diffraction; optical absorption.

1. Introduction

In recent years, kesterite semiconductors Cu_2ZnSnS_4 (CZTS), $Cu_2ZnSnSe_4$ (CZTSe) and $Cu_2ZnSn(S,Se)_4$ (CZTSSe) are being explored as potential alternatives to $Cu(In,Ga)Se_2$ (CIGS) thin film solar cell absorber layer due to their suitable structural, optical and electrical properties as well as their cheaper and abundant constituent elements. So far, the highest reported efficiencies for CZTS, CZTSe and CZTSSe-based thin film solar cells at the laboratory level are 8.4% [1], 9.15% [2] and 12.6% [3], respectively, which are quite low compared with 21.7% [4] of CIGS solar cell. The major issue detrimental for the low device performance in these kesterite solar cells is the low open-circuit voltage, the possible reasons being disorder in the Cu and Zn sites in the CZTS structure [5], existence of band tails due to the potential fluctuations [6], presence of multiple phases [7], etc. The variations in the band gap, deviations in the elemental composition, inhomogeneous grain growth of the films and segregation of ZnS at Mo and CZTS interface [8,9] are also some factors limiting the device efficiency. Hence, optimization of the growth conditions, control of secondary phases, composition, interface properties, etc., is quite necessary to enhance the device performance.

Among kesterite semiconductors, CZTS, with its direct band gap (1.45 eV), high optical absorption coefficient ($\alpha > 10^4$ cm^{-1}) and p-type conductivity, has been explored extensively. Various physical vapour and chemical deposition techniques have been used to prepare CZTS thin films. An approach widely used among these is a two-stage process, wherein the desired precursor layer is co-deposited or precursor layers are sequentially deposited to form a stack using techniques like thermal evaporation [10,11], electron beam evaporation [12,13], DC sputtering [14], RF sputtering/co-sputtering [15,16], hybrid sputtering [17], sequential electrodeposition (ED) [18,19], co-ED [20–22], sol–gel [23–25], SILAR [26], drop casting [27,28], etc., and subsequently, annealing/sulphurizing the same at temperatures in the range 500–600°C in sulphur or H_2S ambience, with nitrogen or argon as the carrier gas in a two-zone furnace or in a graphite box. Sequential deposition of precursors followed by sulphurization is preferred from the point of enhancing the process throughput.

This paper reports the influence of substrate temperature chosen for precursor deposition as well as (N_2+S_2) pressure chosen during annealing on the growth of CZTS films by a two-stage process. Substrate temperature higher than room temperature (RT) is expected to promote easy intermixing/diffusion of these layers in the stack, improve the solid state reaction and enhance grain growth and homogeneity. But too high a substrate temperature leads to re-evaporation of some products. Hence, optimization of T_S is

necessary and is taken as one objective of the present study. Similarly, pressure during sulphurization/annealing is another important process parameter to reduce the re-evaporation losses and obtain films with better microstructure. This is another aspect of the present work.

2. Experimental

ZnS (99.99%), Sn (99.95%) and Cu (99.999%) (all from Sigma-Aldrich) precursor layers were deposited sequentially onto soda–lime glass substrates in a box-type vacuum coating unit (Hind High Vacuum Private Ltd, India, Model: BC-300). Prior to deposition, the substrates were cleaned chemically and ultrasonically; this was followed by ion bombardment in the vacuum chamber. Each evaporation source was pre-calibrated using a quartz crystal thickness monitor to get the desired evaporation rate and thickness. The base and working pressures of the vacuum chamber were 4×10^{-6} and 5×10^{-5} mbar, respectively. To achieve uniformity all over the substrates, the substrate holder was rotated using a rotary drive mechanism. Precursor stack, ZnS–Sn–Cu, was deposited at three different substrate temperatures (T_S), viz., RT, 300 and 400°C, to study the effect of T_S. The stack sequence was chosen to be ZnS–Sn–Cu since Cu acts as a capping layer, minimizes re-evaporation of Sn, diffuses faster and quickly reacts with Sn, forming Cu–Sn intermetallics. Adhesion is found to be better with ZnS as the bottom layer. The thicknesses of ZnS (250 nm), Sn (130 nm) and Cu (100 nm) were so chosen to obtain Cu-poor and Zn-rich CZTS films, preferred for device fabrication.

In the second stage, ZnS–Sn–Cu stacks were annealed at 550°C in sulphur atmosphere separately in a two-zone tubular quartz furnace for diffusion and reaction to occur for the formation of CZTS. Elemental sulphur (99.998%, Sigma-Aldrich, USA), kept in a Mo boat in a zone, was used as the sulphur source. The stacks were slowly heated at the rate of 20°C min^{-1} up to 300°C and then at the rate of 5°C min^{-1} to 550°C. Concurrently, sulphur temperature was also increased at the rate of 4°C min^{-1} to 130°C to ensure that its vapours are available when the sample reaches a temperature of 350°C to reduce the Zn–Sn losses. Nitrogen was used as the carrier gas and (N_2+S_2) pressure was adjusted to be 10 mbar in one set of experiments and 100 mbar in another set of experiments. Upon reaching the desired annealing temperature of 550°C, the stacks were annealed for 90 min to promote CZTS formation. Then the samples were cooled at the rate of 5°C min^{-1} down to 250°C, during which period sulphur source temperature was maintained at 130°C. Afterwards, the samples were cooled naturally to RT.

Crystal structure analysis of the films is carried out by recording X-ray diffraction (XRD) patterns on a BRUKER diffractometer (D8 Advance) with Cu K-α radiation (λ = 0.15406 nm) in the 2θ range 10−60°. Raman spectra were recorded on a Horiba Jobin Yvon HR 800UV confocal micro-Raman spectrometer using a grating with 1800 lines mm^{-1} and Nd–YAG laser source (λ = 532 nm, 20 mW), the spot diameter being ∼1 μm. Carl Zeiss field emission scanning electron microscope (FESEM, Model: ULTRA-55) was used to know the microstructure and an energy dispersive spectrometer (EDS) (Oxford Instruments, UK) attached to it was used to determine the composition. Perkin-Elmer UV–Vis–NIR double-beam spectrophotometer (Model: LAMDA 950) was used to record spectral transmittance and reflectance in the wavelength range 300−2500 nm. Electrical resistivity of the films was determined by the four-probe technique.

3. Results and discussion

3.1 *Composition*

Elemental composition of CZTS films grown by annealing the stacks ZnS–Sn–Cu deposited at different T_S under 10 and 100 mbar pressures is shown in table 1. The uncertainty in the determination of composition data is ±5 at%.

The first three rows correspond to the composition of the film grown under 10 mbar pressure and the next three rows correspond to the composition of films formed under 100 mbar pressure. The films are mostly Cu-poor. Slight Zn-excess and Sn-deficiency are noticed in case of films grown by annealing the stack deposited at T_S = 400°C. With increase

Table 1. Composition of films grown by annealing the stacks deposited at RT, 300 and 400°C under 10 and 100 mbar pressures for 90 min.

T_S (°C)	(N_2+S_2) pressure (mbar)	Composition (at%)				Ratio		
		Cu	Zn	Sn	S	Cu/(Zn+Sn)	Zn/Sn	S/M
RT	10	22.8	12.6	13.4	51.2	0.88	0.94	1.04
300	10	22.5	13.4	13.1	51.0	0.85	1.02	1.04
400	10	20.9	16.3	11.7	51.1	0.75	1.39	1.04
RT	100	22.3	13.2	13.0	51.5	0.85	1.02	1.06
300	100	22.8	13.4	12.8	51.0	0.87	1.05	1.04
400	100	21.0	15.7	12.1	51.2	0.76	1.30	1.05

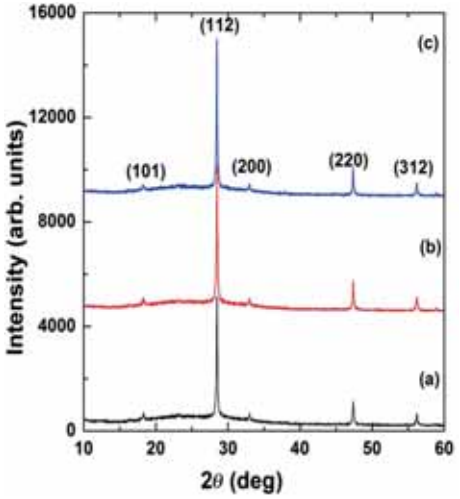

Figure 1. XRD patterns of CZTS films grown by annealing the stacks deposited at (a) RT, (b) 300°C and (c) 400°C under 10 mbar pressure.

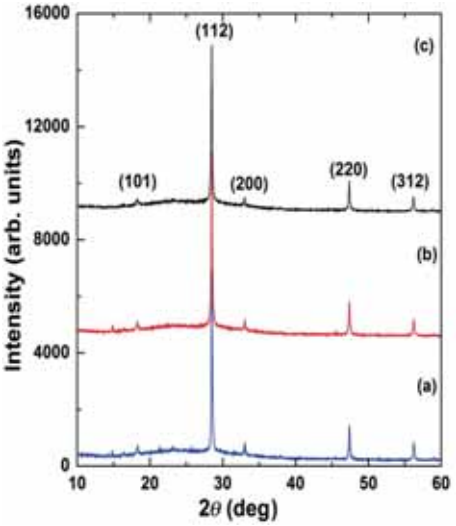

Figure 2. XRD patterns of CZTS films grown by annealing the stacks deposited at (a) RT, (b) 300°C and (c) 400°C under 100 mbar pressure.

in T_S, Sn atomic percentage decreased slightly and Zn atomic percentage slightly increased. Cu/(Zn+Sn) ratio is found to decrease slightly, while Zn/Sn ratio is found to increase slightly with increase in T_S, indicating higher Sn-loss. In case of films deposited at T_S = RT and 300°C, Cu/(Zn+Sn) ratio was close to the targeted value 0.85 but the Zn/Sn ratio deviated from the targeted value of 1.2. CZTS films grown by annealing the stack deposited at 400°C might contain ZnS as the secondary phase, since Zn at% is slightly higher.

3.2 *Structural analysis*

3.2a *XRD analysis*: Figure 1 shows the XRD patterns of films grown by annealing the stacks deposited at RT, 300 and 400°C under 10 mbar pressure. The observed diffraction peaks agree with kesterite CZTS structure (JCPDS card number 26-0575), the preferred orientation being (112). The lattice parameters '*a*' and '*c*' are found to be 0.542 and 1.082 nm, respectively. The slight decrease in the full-width at half-maximum (FWHM) of the peaks with increase in T_S indicates a slight improvement in crystallinity. The crystallite size, evaluated from Scherrer's formula [29], is found to be 60, 65 and 70 nm for films grown by annealing the stacks deposited at RT, 300 and 400°C, respectively. The presence of binary sulphides of Cu and Sn as well as ternary phases like Cu_3SnS_4 and Cu_4SnS_4 is ruled out as their strongest diffraction peaks are absent. However, it is difficult to conclude about the presence/absence of ZnS and Cu_2SnS_3 (CTS) phases from the present analysis as their intense diffraction peaks are quite close to those of CZTS.

XRD patterns of films grown by annealing the stacks deposited at RT, 300 and 400°C under 100 mbar pressure are shown in the figure 2. The diffraction patterns match well with kesterite CZTS, the preferred orientation being (112).

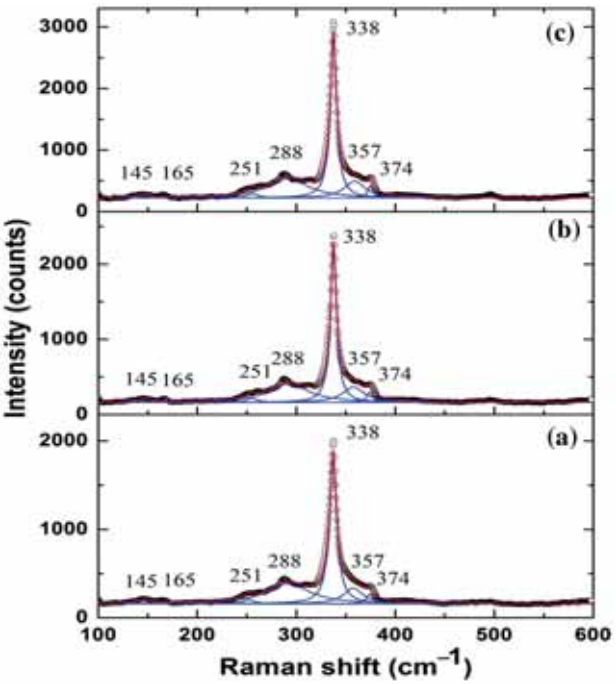

Figure 3. Raman spectra of CZTS films grown by annealing the stacks deposited at (a) RT, (b) 300°C and (c) 400°C under 10 mbar pressure.

The crystallite size is found to be 65, 70 and 75 nm, respectively, for films obtained on annealing the stacks deposited at RT, 300 and 400°C. Crystallite size of these films is slightly greater than that of films grown under 10 mbar pressure.

3.2b *Raman spectroscopy analysis*: Raman spectra is used to know the presence of CTS and ZnS phases. Figure 3 shows the micro-Raman spectra of films grown by annealing

the stacks deposited at T_S = RT, 300 and 400°C under 10 mbar pressure. In all these spectra, the most intense mode is at 338 cm^{-1} with other modes at 145, 165, 251, 288, 357 and 374 cm^{-1}. The most intense mode at 338 cm^{-1} as well as weaker modes at 288 and 374 cm^{-1} are due to CZTS and are in agreement with the reported Raman modes of CZTS at 336−339, 287−288 and 368−374 cm^{-1} [10,30–34]. The broad humps at 145, 165 and 251 cm^{-1} and a shoulder at 357 cm^{-1} to the most intense peak are also close to the reported CZTS Raman modes [35–37]. The intensity of the observed Raman modes is found to increase with T_S. The FWHM of the most intense peak is found to decrease from 7.5 to 6.0 cm^{-1} with increase in T_S, indicating a slight improvement in crystallinity. The reported FWHM of the most intense Raman mode of CZTS thin films is in the range 2.0−14.0 cm^{-1} [10,30–37].

Coming to the detection of the secondary phase CTS, if any, its reported Raman data are used for analysis. CTS is reported to be polymorphic and can crystallize in cubic, tetragonal, monoclinic and triclinic structures [38,39]. The Raman modes for tetragonal CTS phase were reported to occur at 336, 297 and 352 cm^{-1} [38]. The most intense mode observed at 338 cm^{-1} in the present case is close to the most intense mode of tetragonal CTS phase at 336 cm^{-1}. But the absence of the other two equally intense modes at 297 and 352 cm^{-1} reported for this phase [38] in the present case (figure 3) rules out its possibility. Similarly, cubic CTS phase is not expected as its intense mode reported at 303 cm^{-1} [38] is absent in the spectra (figure 3). Raman modes due to monoclinic CTS phase were reported to occur at 292 and 350 cm^{-1} [39]. From our recent studies [40] on co-evaporated CTS thin films deposited at T_S = 350°C and annealed at 550°C, we found that the

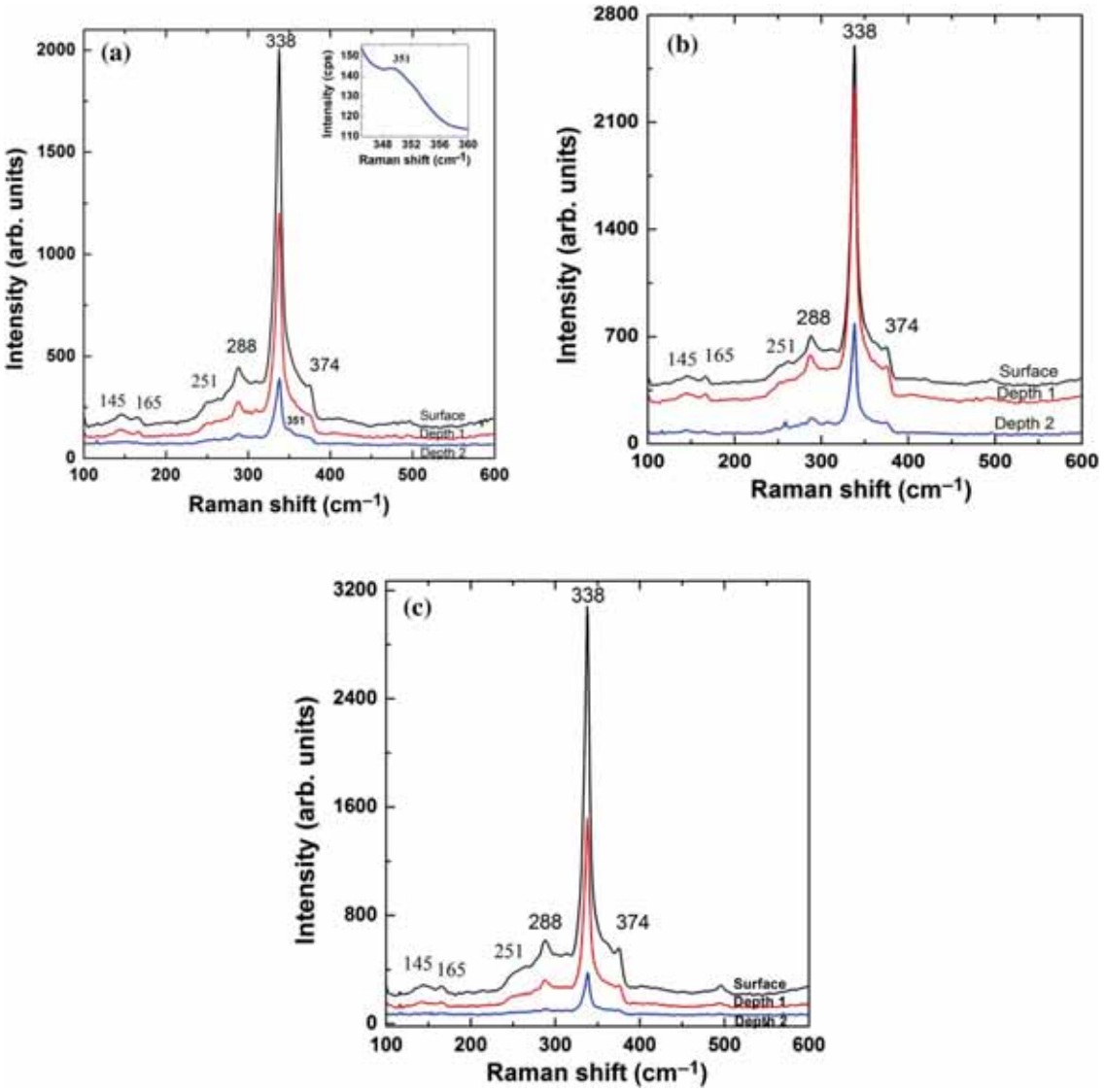

Figure 4. Raman depth profiles of CZTS films grown by annealing the stacks deposited at (**a**) RT, (**b**) 300°C and (**c**) 400°C under 10 mbar pressure.

dominant phase under these growth conditions is monoclinic CTS phase with two equally intense modes at 290 and 349 cm^{-1}, in agreement with published data [39]. The low intense mode at 288 cm^{-1} and a broad hump in the region 350−374 cm^{-1} in the Raman spectra (figure 3) of films suggest that a minute monoclinic CTS phase might be present but the very low intensity of these modes and their close overlap with the weak modes of CZTS makes it difficult to conclude affirmatively.

With regard to the detection of ZnS, another structurally close phase, its strongest Raman mode is expected at 352 cm^{-1} with a weak mode at 275 cm^{-1} [32,41,42]. The hump in the region 350−374 cm^{-1} is broad and its intensity being low, it is difficult to conclude the presence of ZnS phase, since CZTS has also a weak mode in this region. We could not record Raman spectra with 325 nm laser excitation to ascertain the presence of ZnS, as was done by some groups, due to lack of this facility at our end and also access time constraints for us at neighbouring institutes. But EDS analysis showed that the films grown on annealing the stack deposited at 400°C are slightly Zn-rich and thus ZnS might be present minutely in these films.

In order to know whether the films are depth-wise homogeneous, Raman spectra (figure 4) were recorded at two different depths by manually moving the sample stage along Z-direction. Figure 4a, corresponding to the films grown on annealing the stack deposited at RT, shows a small hump at 352 cm^{-1} in the depth-2 spectrum (magnified portion shown in the inset), indicating the presence of a small quantity of ZnS [32,41,42] close to the substrate. This feature is not perceivable in figure 4b and c, corresponding to the films grown on annealing the stacks deposited, respectively, at 300 and 400°C.

Raman spectra of films grown by annealing the stacks (deposited at RT, 300 and 400°C) under 100 mbar pressure are shown in figure 5. The intense Raman modes of CZTS at 338, 288 and 375 cm^{-1} can be seen in addition to other broad humps at 143, 166, 251 and 357 cm^{-1}. The FWHM of the most intense Raman mode in all these cases is ∼6 cm^{-1} and is slightly lesser than the FWHM of the Raman modes of the films obtained on annealing the stacks under 10 mbar pressure. Other than this, no significant differences in Raman spectra of films grown on annealing the stacks under 10 mbar (figure 3) and 100 mbar (figure 5) pressures can be seen. Perceivable changes in the spectra with depth could not be observed even in this case.

3.3 *Microstructure*

Figure 6 shows the scanning electron micrographs of the films grown by annealing the stacks deposited at RT, 300 and 400°C under 10 mbar pressure. The micrograph of films grown by annealing the stack deposited at T_S = RT (figure 6a) shows a large number of nearly round-shaped grains (marked A) with a very few elongated large grains (marked B). A few broken-bubble-like areas, comprising round shaped grains

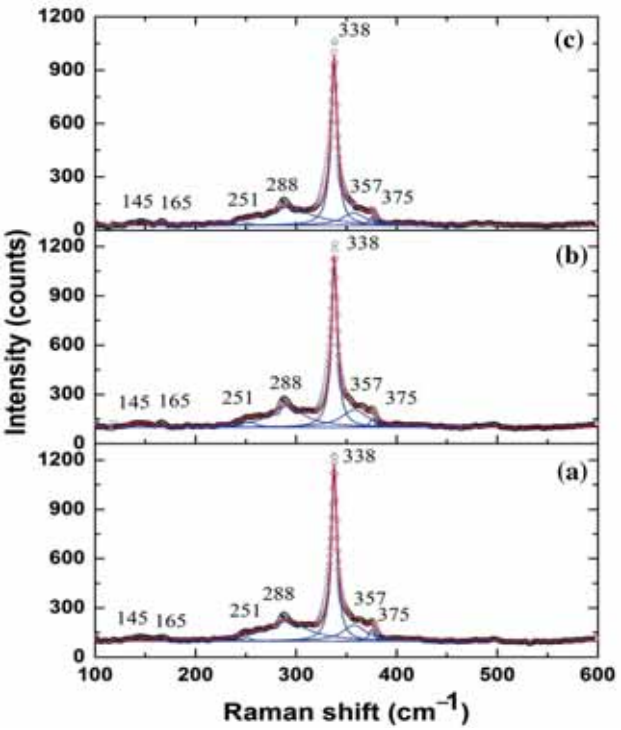

Figure 5. Raman spectra of CZTS films grown by annealing the stacks deposited at (a) RT, (b) 300°C and (c) 400°C under 100 mbar pressure.

(marked A), can also be seen. These broken areas might be due to eruption on annealing of hemisphere-shaped intermetallic (Cu–Sn) grains formed during the deposition. This inference is based on our observation of the morphology (not shown) of as-deposited ZnS–Sn–Cu stacks prior to annealing, with hemisphere-shaped grains similar to the reported morphology [13] of films when there is formation of Cu–Sn intermetallic.

The microstructure of films grown by annealing the stack deposited at 300°C (figure 6b) is more distinct and compact with increase in the number of large grains (marked B) interspaced with fine crystallite regions (marked C). The grain size varies from ∼50 to ∼500 nm. Erupted bubble-like areas, observed in the earlier case, are present to a lesser extent. The microstructure of films grown by annealing the stack deposited at 400°C (figure 6c) shows further enhancement in grain size and a few crater-like regions are seen probably due to surface decomposition.

Figure 7 shows scanning electron micrographs of films grown by annealing the stacks deposited at RT, 300 and 400°C under 100 mbar pressure. The micrograph of films grown by annealing the stacks deposited at RT shows (figure 7a) grains with different morphologies and contrast: a few small round-shaped grain regions (marked A), a few large grains (marked B), a few very fine crystallites (marked C) and very few hexagon-shaped grains (marked D). Comparing this with the corresponding microstructure (figure 6a) of films grown by annealing under 10 mbar pressure, it is seen that the small round-shaped crystallites (marked A) in figure 7a are similar

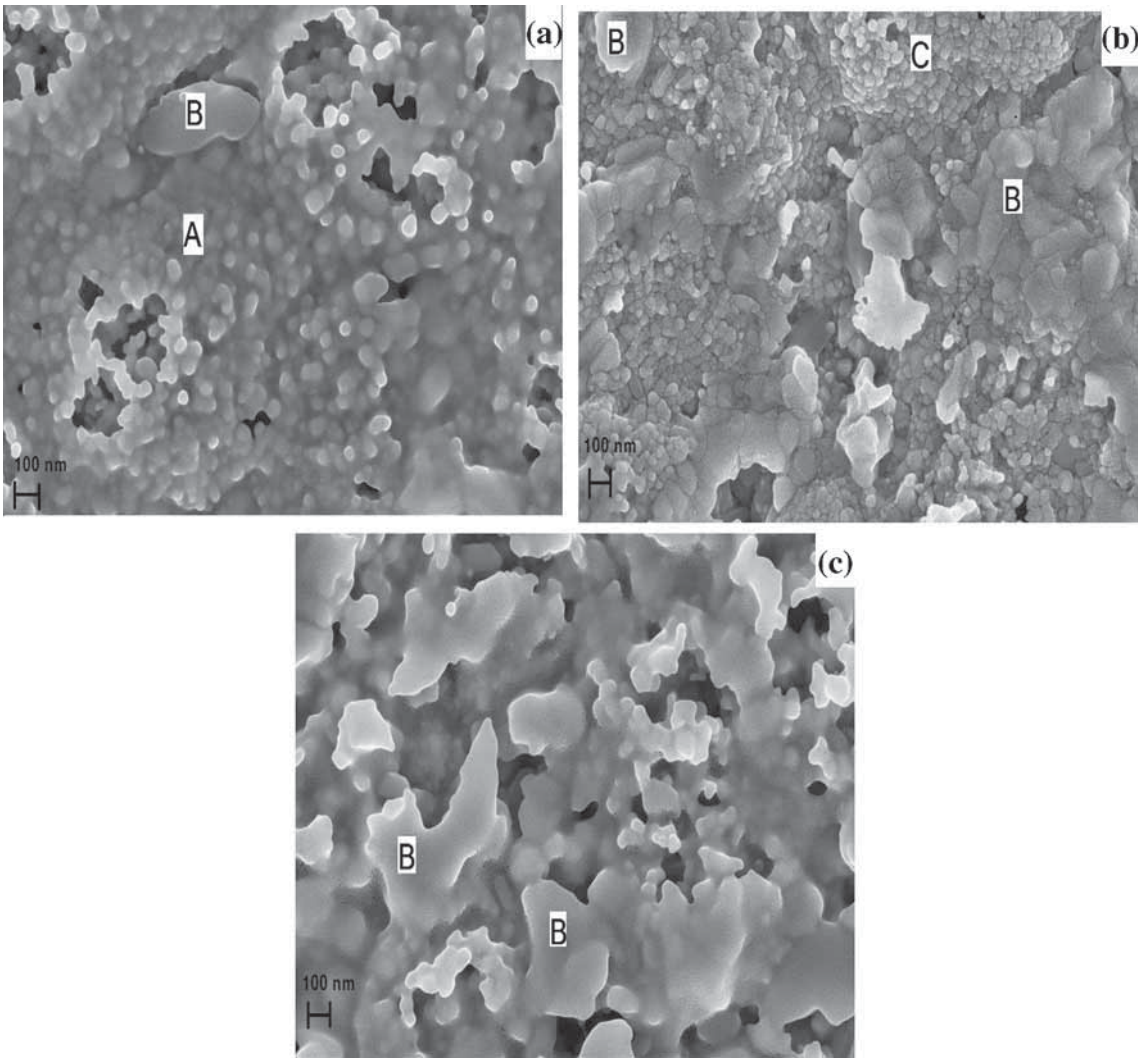

Figure 6. Scanning electron micrographs of CZTS films grown by annealing the stacks deposited at (**a**) RT, (**b**) 300°C and (**c**) 400°C under 10 mbar pressure.

to the region A in figure 6a and their extent decreased with increase in the annealing pressure. The large grains (marked B) seen in figure 6a are also present in figure 7a, but to a larger extent in the latter. Regions marked C in figure 7a and hexagon-shaped grains (marked D) are not seen in the micrograph of the films obtained under 10 mbar pressure. The hexagon-shaped crystallites might be those of copper sulphide [43]. XRD and Raman analyses of the films obtained on annealing under 100 mbar pressure did not reveal the presence of copper sulphide probably due to its minute content below the detection limit. EDS analysis of the chosen grains/regions, or line scan as was done by some groups [10,33,35,44] to know what these regions are, could not be carried out due to FESEM access time constraints.

Comparing the microstructure (figures 6b and 7b) of the films grown by depositing the stacks at 300°C and annealing the same under 10 and 100 mbar pressures, it is observed that the fine crystallite regions (marked C), observed in figure 6b, decreased to a considerable extent with improvement in the large grain formation (marked B), when annealed under 100 mbar pressure. The microstructure of films (figure 7c) obtained on annealing the stack deposited at 400°C shows more void regions due to re-evaporation. Thus the deposition of the stack at 400°C does not lead to good films in any way.

3.4 *Optical absorption*

Figure 8 shows the transmittance (T_λ) and reflectance (R_λ) curves of films grown by annealing the stacks deposited at T_S = RT, 300 and 400°C under 10 mbar pressure. The spectral transmittance of the films is found to increase with an increase in T_S. Interference maxima and minima in these curves reveal that the films are specular. The slight shift in positions of reflectance minima/maxima and transmittance maxima/minima might be due to some inhomogeneities in

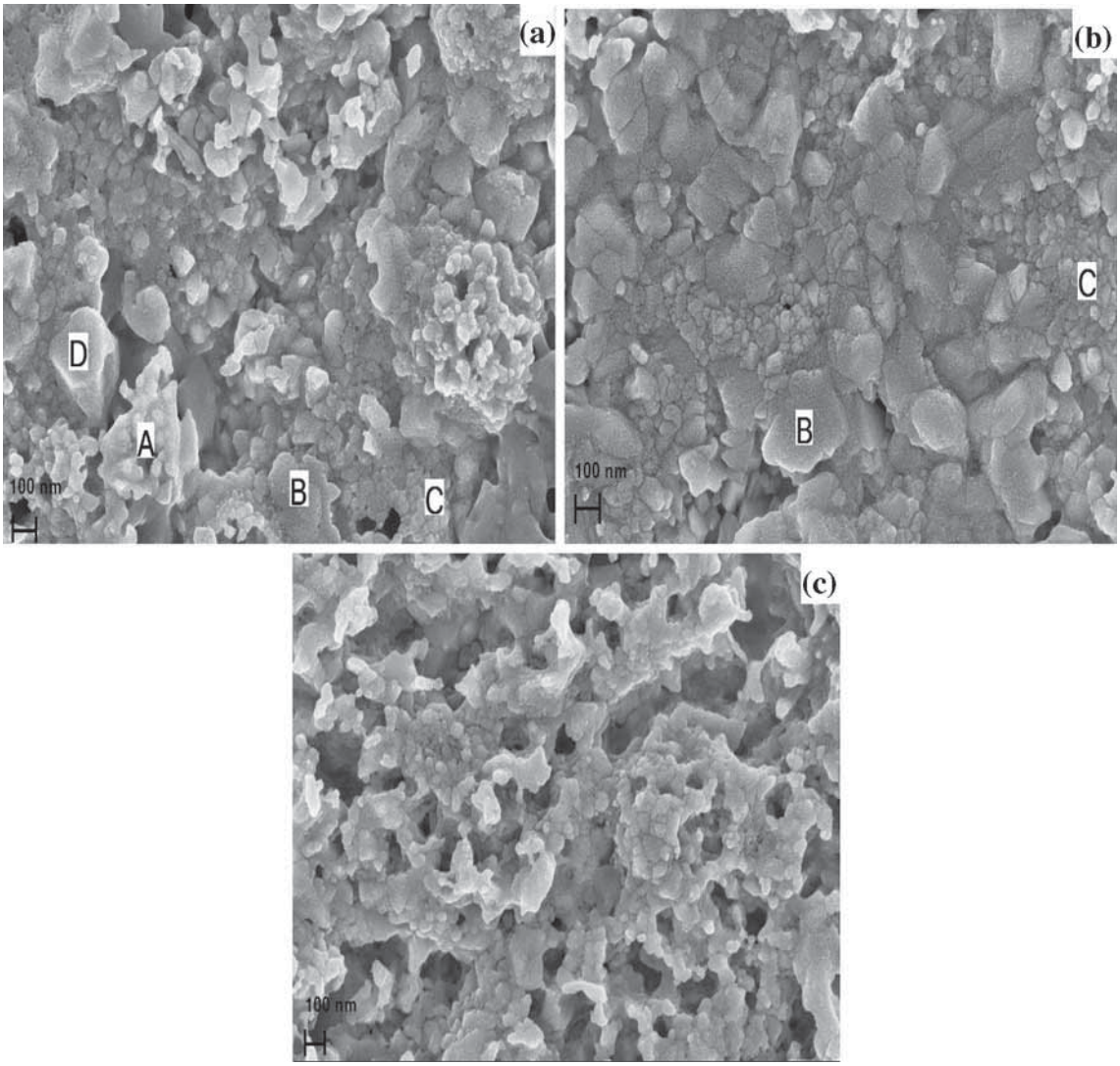

Figure 7. Scanning electron micrographs of CZTS films grown by annealing the stacks deposited at (**a**) RT, (**b**) 300°C and (**c**) 400°C under 100 mbar pressure.

the films. The onset of fundamental absorption edge commences at ∼950 nm, as seen from the decrease of T_λ and R_λ. The slight difference in the wavelength of onset among these films is probably due to the variation in crystallinity and/or composition. Also, simultaneous decrease in transmittance and reflectance for $\lambda < \sim 750$ nm suggests an additional absorption process, which might be due to binary phases like ZnS or Cu_xS. Very low intensity in this region and the minute presence of ZnS phase, if any, make the assignment difficult. Based on Raman spectra analysis presented in Section 3.2a, an affirmative conclusion about the presence/absence of monoclinic CTS phase could not be drawn. However, if the monoclinic CTS phase is present, its fundamental absorption edge is expected at ∼1500 nm [40] and its absence in figure 8 rules out the presence of monoclinic CTS phase in these films. The observed fundamental absorption edge at ∼950 nm is due to CZTS phase and is in agreement with reported trend in literature.

From the transmittance and reflectance data, optical absorption coefficient (α_λ) is calculated using the equation $\alpha_\lambda = \ln((1 - R_\lambda)^2/T_\lambda)/t$, where '$t$' is the film thickness.

The average thickness of these films is ∼0.6 μm. The nature of the optical transition, whether direct or indirect, and band gap are determined from the equation $\alpha h\nu = A(h\nu - E_g)^n$. Here '$A$' is a constant and '$n$' depends on the type of transition; 'n' can take a value of 1/2, 2, 3/2 or 3 based on whether the transition is direct-allowed, indirect-allowed, direct-forbidden or indirect-forbidden, respectively. In the present study, this equation is found to be satisfied for $n = 1/2$, indicating that the optical transitions are direct-allowed in nature. The band gap is evaluated by extending the linear fit region of $(\alpha h\nu)^2$ *vs.* $h\nu$ plot onto $h\nu$-axis.

Figure 9 shows $(\alpha h\nu)^2$ *vs.* $h\nu$ curves of CZTS films grown by annealing the stacks deposited at RT, 300 and 400°C under 10 mbar pressure. The direct optical band gaps of CZTS films grown by annealing the stacks deposited at RT, 300 and 400°C

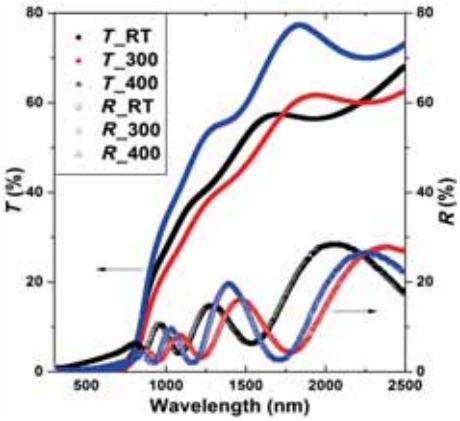

Figure 8. Transmittance (T_λ) and reflectance (R_λ) curves of CZTS films grown by annealing the stacks deposited at (a) RT, (b) 300°C and (c) 400°C under 10 mbar pressure.

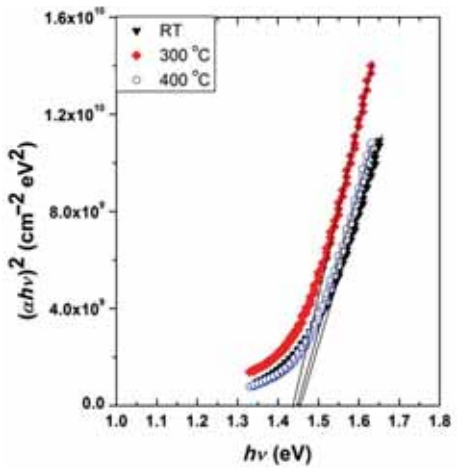

Figure 9. $(\alpha h\nu)^2$ *vs.* $h\nu$ plots of CZTS films grown by annealing the stacks deposited at RT, 300 and 400°C under 10 mbar pressure.

are 1.46, 1.44 and 1.45 eV, respectively. The error in the evaluation of the band gap is ±0.02 eV. The observed values are close to the reported CZTS band gap of 1.45 eV [13,23].

Figure 10 shows transmittance (T_λ) and reflectance (R_λ) curves of films grown by annealing the stacks deposited at RT, 300 and 400°C, under 100 mbar pressure. A slight increase in the transmittance for wavelengths <1250 nm and steeper fundamental absorption edge are observed compared with the spectra of films grown under 10 mbar pressure. Figure 11 shows the $(\alpha h\nu)^2$ *vs.* $h\nu$ curves of films grown by annealing the stacks under 100 mbar pressure. The band gap values of these films are found to be 1.45, 1.45 and 1.48 eV, correspondingly.

3.5 *Electrical resistivity*

RT electrical resistivities of films grown by annealing the stacks deposited at RT, 300 and 400°C under 10 mbar pressure were found to be 55, 40 and 25 Ω cm, respectively. For

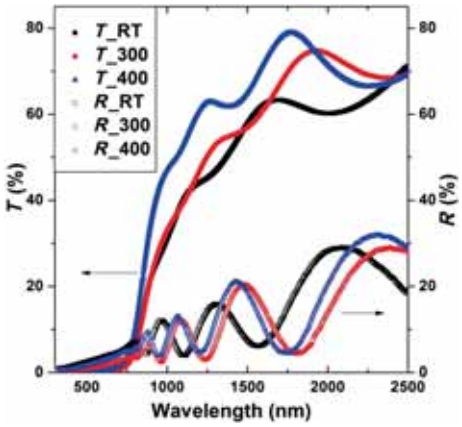

Figure 10. Transmittance (T_λ) and reflectance (R_λ) curves of CZTS films grown by annealing the stacks deposited at RT, 300 and 400°C under 100 mbar pressure.

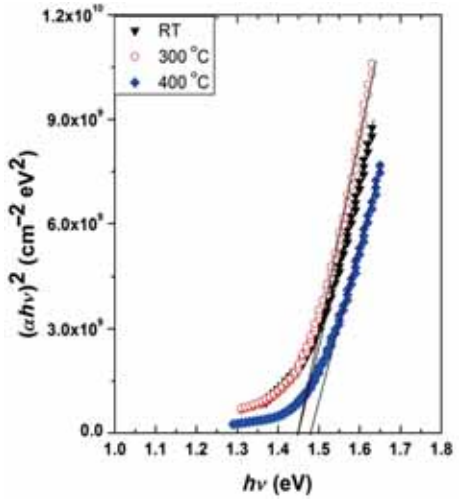

Figure 11. $(\alpha h\nu)^2$ *vs.* $h\nu$ plots of CZTS films grown by annealing the stacks deposited at RT, 300 and 400°C under 100 mbar pressure.

films grown under 100 mbar pressure, it is found to be 25, 10 and 5 Ω cm, correspondingly, for the same T_S sequence. The slight decrease in resistivity of the films with increase in T_S as well as pressure during annealing might be due to the improvement in crystallinity.

4. Conclusions

Cu-poor, Zn-rich CZTS films were grown by a two-stage process. The effects of substrate temperature used for the deposition of the precursors and (N_2+S_2) pressure during annealing on the structural, microstructural and optical properties of CZTS films are investigated. The films exhibited kesterite structure with (112) preferred orientation. The lattice parameters '*a*' and '*c*' are found to be 0.542 and 1.082 nm, respectively. The crystallite size is found to increase from 60 to 70 nm with increase in T_S. Raman spectra analysis also confirmed this trend as observed from the decrease in FWHM of

the most intense Raman mode of CZTS from 7.5 to 6.0 cm^{-1} with increase in T_S. The direct band gap of these films is found to be ∼1.45 eV. RT electrical resistivity is found to decrease with increase in T_S due to improvement in crystallinity. The crystallinity of the films is also found to increase with increase in pressure during annealing from 10 to 100 mbar. The influence of T_S and (N_2+S_2) pressure chosen for subsequent annealing to obtain CZTS films is clearly perceivable, especially in microstructure. The films grown by annealing the stacks deposited at 300°C under 100 mbar pressure are found to have compact microstructure with large grains interspaced with fine crystallite regions. However, the films grown by depositing precursors at 400°C showed poor microstructure with voids. Thus, substrate temperature of 300°C and (N_2+S_2) pressure of 100 mbar during annealing are considered as optimal in this two-stage process to achieve Cu-poor and Zn-rich CZTS films with compact grain morphology.

Acknowledgements

Dr U Chalapathi expresses his grateful thanks to the University Grants Commission (UGC), New Delhi, for providing BSR fellowship grant to carry out this research. The timely help by School of Physics, University of Hyderabad, Hyderabad, for extending FESEM services is gratefully acknowledged.

References

[1] Shin B, Gunawan O, Zhu Y, Bojarczuk N A, Jay Chey S *et al* 2013 *Prog. Photovolt.: Res. Appl.* **21** 72
[2] Repins I, Beall C, Ora N, DeHart C, Kuciauskas D, Dippo P *et al* 2012 *Sol. Energy Mater. Sol. Cells* **101** 154
[3] Wang W, Winkler M T, Gunawan O, Gokmen T, Todorov T K, Zhu Y *et al* 2014 *Adv. Energy Mater.* **4** 130146
[4] Jackson P, Hariskos D, Wuerz R, Kiowski O, Bauer A, Friedlmeier T M *et al* 2014 *Phys. Status Solidi (RRL)* **9999** 28
[5] Scragg J J, Choubrac L, Lafond A, Ericson T and Platzer-Bjorkman C 2014 *Appl. Phys. Lett.* **104** 041911
[6] Gershon T, Shin B, Gokmen T, Lu S, Bojarczuk N and Guha S 2013 *Appl. Phys. Lett.* **103** 193903
[7] Djemour R, Redinger A, Mousel M, Gütay L and Siebentritt S 2014 *J. Appl. Phys.* **116** 073509
[8] Malerba C, Biccari F, Ricardo C L A, Valentini M, Chierchia R, Müller M *et al* 2014 *J. Alloys Compd.* **582** 528
[9] Li W, Chen J, Yan C and Hao X 2015 *J. Alloys Compd.* **632** 178
[10] Cheng A J, Manno M, Khare A, Leighton C, Campbell S A and Aydil E S 2011 *J. Vac. Sci. Technol. A* **29** 051203
[11] Chalapathi U, Uthanna S and Sundara Raja V 2015 *Sol. Energy Mater. Sol. Cells* **132** 476
[12] Katagiri H, Saitoh K, Washio T, Shinohara H, Kurumadani T and Miyajima S 2001 *Sol. Energy Mater. Sol. Cells* **65** 141
[13] Araki H, Mikaduki A, Kubo Y, Sato T, Jimbo K, Maw W S *et al* 2008 *Thin Solid Films* **517** 1457
[14] Fernandes P, Salomé P and da Cunha A 2009 *Semicond. Sci. Technol.* **24** 105013
[15] Yoo H and Kim J 2010 *Thin Solid Films* **518** 6567
[16] Momose N, Htay M T, Yudasaka T, Igarashi S, Seki T, Iwano S *et al* 2011 *Jpn. J. Appl. Phys.* **50** 01BG09
[17] Tanaka T, Nagatomo T, Kawasaki D, Nishio M, Guo Q, Wakahara A *et al* 2005 *J. Phys. Chem. Solids* **66** 1978
[18] Scragg J J, Dale P J and Peter L M 2009 *Thin Solid Films* **517** 2481
[19] Araki H, Kubo Y, Mikaduki A, Jimbo K, Maw W S, Katagiri H *et al* 2009 *Sol. Energy Mater. Sol. Cells* **93** 996
[20] Schurr R, Hölzing A, Jost S, Hock R, Voβ T, Schulze J *et al* 2009 *Thin Solid Films* **517** 2465
[21] Ennaoui A, Lux-Steiner M, Weber A, Abou-Ras D, Kötschau I, Schock H W *et al* 2009 *Thin Solid Films* **517** 2511
[22] He X, Shen H, Wang W, Pi J, Hao Y and Shi X 2013 *Appl. Surf. Sci.* **282** 765
[23] Tanaka K, Moritake N and Uchiki H 2007 *Sol. Energy Mater. Sol. Cells* **91** 1199
[24] Maeda K, Tanaka K, Nakano Y and Uchiki H 2011 *Jpn. J. Appl. Phys.* **50** 05FB08
[25] Zhang K, Su Z, Zhao L, Yan C, Liu F, Cui H *et al* 2014 *Appl. Phys. Lett.* **104** 141101
[26] Su Z, Yan C, Sun K, Han Z, Liu F, Liu J *et al* 2012 *Appl. Surf. Sci.* **258** 7678
[27] Guo Q, Hillhouse H W and Agrawal R 2009 *J. Am. Chem. Soc.* **131** 11672
[28] Samji S K, Tiwari B, Surendra M K and Rao M R 2014 *Appl. Phys. Lett.* **104** 152106
[29] Cullity B D 1956 *Elements of X-ray diffraction* (London: Addison Wesley)
[30] Himmrich M and Haeuseler H 1991 *Spectrochim. Acta A: Mol. Spectrosc.* **47** 933
[31] Altosaar M, Raudoja J, Timmo K, Danilson M, Grossberg M, Krustok J *et al* 2008 *Phys. Status Solidi A* **205** 167
[32] Fernandes P A, Salome P M P and da Cunha A F 2011 *J. Alloys Compd.* **509** 7600
[33] Wang K, Shin B, Reuter K B, Todorov T, Mitzi D B and Guha S 2011 *Appl. Phys. Lett.* **98** 051912
[34] Yoo H and Kim J 2011 *Sol. Energy Mater. Sol. Cells* **95** 239
[35] Fontané X, Calvo-Barrio L, Izquierdo-Roca V, Saucedo E, Pérez-Rodriguez A, Morante J R *et al* 2011 *Appl. Phys. Lett.* **98** 181905
[36] Fontané X, Izquierdo-Roca V, Saucedo E, Schorr S, Yukhymchuk V, Valakh M Y *et al* 2012 *J. Alloys Compd.* **539** 190
[37] Dumcenco D and Huang Y S 2012 *Opt. Mater.* **35** 419
[38] Fernandes P A, Salome P M P and da Cunha A F 2010 *J. Phys. D: Appl. Phys.* **43** 215403
[39] Berg D M, Djemour R, Gutay L, Siebentritt S, Dale P J, Fontane X *et al* 2012 *Appl. Phys. Lett.* **100** 192103
[40] Chalapathi U, Jayasree Y, Uthanna S and Raja V S 2015 *Vacuum* **117** 121
[41] Nilsen W 1969 *Phys. Rev.* **182** 838
[42] Fernandes P A, Salome P M P and da Cunha A F 2009 *Thin Solid Films* **517** 2519
[43] Dhasade S S, Patil J S, Kim J H, Han S H, Rath M C and Fulari V J 2012 *Mater. Chem. Phys.* **137** 353
[44] Scragg J J, Ericson T, Fontané X, Izquierdo-Roca V, Pérez-Rodriguez A, Kubart T *et al* 2014 *Prog. Photovolt.: Res. Appl.* **22** 10